A New Perspective on Southern Hemisphere Storm Tracks

B. J. HOSKINS

Department of Meteorology, University of Reading, Reading, United Kingdom

K. I. HODGES

Environmental Systems Science Centre, University of Reading, Reading, United Kingdom

(Manuscript received 28 October 2004, in final form 11 May 2005)

ABSTRACT

A detailed view of Southern Hemisphere storm tracks is obtained based on the application of filtered variance and modern feature-tracking techniques to a wide range of 45-yr European Centre for Medium-Range Weather Forecasts (ECMWF) Re-Analysis (ERA-40) data. It has been checked that the conclusions drawn in this study are valid even if data from only the satellite era are used. The emphasis of the paper is on the winter season, but results for the four seasons are also discussed. Both upper- and lower-tropospheric fields are used. The tracking analysis focuses on systems that last longer than 2 days and are mobile (move more than 1000 km). Many of the results support previous ideas about the storm tracks, but some new insights are also obtained. In the summer there is a rather circular, strong, deep high-latitude storm track. In winter the high-latitude storm track is more asymmetric with a spiral from the Atlantic and Indian Oceans in toward Antarctica and a subtropical jet–related lower-latitude storm track over the Pacific, again tending to spiral poleward. At all times of the year, maximum storm activity in the higher-latitude storm track is in the Atlantic and Indian Ocean regions. In the winter upper troposphere, the relative importance of, and interplay between, the subtropical and subpolar storm tracks is discussed. The genesis, lysis, and growth rate of lower-tropospheric winter cyclones together lead to a vivid picture of their behavior that is summarized as a set of overlapping plates, each composed of cyclone life cycles. Systems in each plate appear to feed the genesis in the next plate through downstream development in the upper-troposphere spiral storm track. In the lee of the Andes in South America, there is cyclogenesis associated with the subtropical jet and also, poleward of this, cyclogenesis largely associated with system decay on the upslope and regeneration on the downslope. The genesis and lysis of cyclones and anticyclones have a definite spatial relationship with each other and with the Andes. At 500 hPa, their relative longitudinal positions are consistent with vortex-stretching ideas for simple flow over a large-scale mountain. Cyclonic systems near Antarctica have generally spiraled in from lower latitudes. However, cyclogenesis associated with mobile cyclones occurs around the Antarctic coast with an interesting genesis maximum over the sea ice near 150°E. The South Pacific storm track emerges clearly from the tracking as a coherent deep feature spiraling from Australia to southern South America. A feature of the summer season is the genesis of eastward-moving cyclonic systems near the tropic of Capricorn off Brazil, in the central Pacific and, to a lesser extent, off Madagascar, followed by movement along the southwest flanks of the subtropical anticyclones and contribution to the "convergence zone" cloud bands seen in these regions.

1. Introduction

The storm tracks of the Southern Hemisphere (SH) are important for the weather there and also for climate processes through their latitudinal transports and their driving of the Southern Ocean. This has resulted in many studies of the SH storm tracks. Taljaard (1972) gave an excellent summary of the understanding of the structure of the SH storm tracks obtained over many years but in particular from analysis of extra observations obtained in and following the 1957 International Geophysical Year (IGY). However, there was of course considerably less knowledge available than for the NH, which has been more extensively observed and studied. With the advent of satellite data and routine global analyses, this situation has improved markedly. Streten

Corresponding author address: Kevin I. Hodges, Environmental Systems Science Centre, University of Reading, Harry Pitt Building, 3 Earley Gate, Whiteknights, P.O. Box 238, Reading RG6 6AL, United Kingdom.
E-mail: kih@mail.nerc-essc.ac.uk

and Troup (1973) used early hemispheric composite satellite imagery to subjectively identify and track cloud vortices associated with cyclones and produced a climatology of them. In a later study, Carlton (1981) used a similar approach to study the cyclone activity for the extended winter period. Trenberth (1991) used European Centre for Medium-Range Weather Forecasts (ECMWF) data and standard Eulerian variance and covariance diagnostics to give a detailed zonally averaged view and some discussion of the geographical structure, while Berbery and Vera (1996) used filtered and unfiltered ECMWF data to explore the structure and evolution of synoptic-scale waves.

Cyclone and anticyclone tracking provides a complementary approach to that of the usual Eulerian approach to diagnosing storm-track activity and has played a significant role in SH storm-track research, using not only the satellite imagery but also data from operational analysis and reanalysis. Sinclair (1994, 1995, 1996), for example, identified systems as extrema in the geostrophic vorticity and tracked these to produce a climatology of systems that moved more than 10°. Simmonds and collaborators (e.g., Simmonds and Murray 1999) developed and refined a technique based on sea level pressure minima as identified through maxima in a finite-difference Laplacian and did not impose a movement requirement. In Simmonds and Keay (2000) a climatology of cyclone behavior for the SH was produced using this technique applied to the 40-yr National Centers for Environmental Prediction–National Center for Atmospheric Research (NCEP–NCAR) reanalysis.

Interest in the weather and climate of Antarctica has meant that there have also been a considerable number of studies focusing on the cyclones and mesoscale vortices around its periphery, for example, in recent years the studies based on satellite imagery of Carrasco et al. (2003) and Turner et al. (1998). The importance of katabatic outflow to the genesis and development of these systems has been proposed by Bromwich and Parish (1998) and others.

On the more theoretical side, Mechoso (1980) found that a lower boundary rising toward the pole as in an idealized Antarctic topography acts to reduce baroclinic instability but that this is insufficient to stabilize a westerly "subpolar" jet around the topography forced by waves moving in from lower latitudes. In another study, Frederiksen (1984) determined the growing normal modes for zonally averaged and three-dimensional SH flows and found that structures with comparable growth rates could be centered in the band 40°–45°S or near 60°S, being associated, respectively, with the subtropical or subpolar jets. A wave packet view of Southern Hemisphere cyclone family organization was discussed by Lee and Held (1993) and was further developed by Berbery and Vera (1996). The latter also found consistency between the storm-track locations and the baroclinicity of the mean flow. The strong linking of the Atlantic and Indian Ocean lower-level storm track with large gradients in sea surface temperature (SST) was recently supported by Nakamura and Shimpo (2004). They also emphasized the importance of the strong winter subtropical jet in the Australian sector acting as a waveguide and inhibiting the poleward propagation of wave activity in to the high-latitude storm track in the Pacific. Inatsu and Hoskins (2004), using controlled experiments with an atmospheric GCM confirmed that the zonal asymmetry of SST was crucial for the low-level winter storm-track structure. The topography of South America and South Africa was also influential in this regard. However, they found that the asymmetry of the mean flow and storm track in the upper troposphere was dominated by a stationary Rossby wave forced by the asymmetries in convective heating in the northern Tropics.

In Hoskins and Hodges (2002), 15-yr ECMWF Re-Analysis (ERA-15) data in the Northern Hemisphere (NH) were used to produce Eulerian variances of time-filtered fields for a variety of upper- and lower-tropospheric variables. These where contrasted with results from an objective tracking procedure developed by Hodges (1995, 1996, 1999) and applied to the same fields to give a new perspective on the NH winter storm tracks. The purpose of the present paper is to perform a similar investigation in the SH, based on the 40+ years of 40-yr ECMWF Re-Analysis (ERA-40) data, to provide a new perspective on the SH storm tracks. Discussion of the four seasons will be given, but the concentration here is on the winter season (June–August), which is notable for its zonal asymmetry.

As basic background material for this paper, Fig. 1 summarizes some aspects of the mean summer and winter flow in the SH as given by the ERA-40 dataset, which is discussed below. Shown are summary pictures for the upper and lower troposphere in December–February (DJF, summer; hereafter 3-month periods are denoted by the first letter of each respective month) and JJA (winter). The upper troposphere (Figs. 1a,b) is here characterized by fields on the potential vorticity (PV) surface, PV = +/−2 PVU, where the minus sign applies in the SH. This can be considered to be the dynamical tropopause (Hoskins and Berrisford 1988). Shown are the zonal winds ($\overline{U}_{\mathrm{PV}=2}$) overlaid on the pole-to-equator meridional gradient of potential tem-

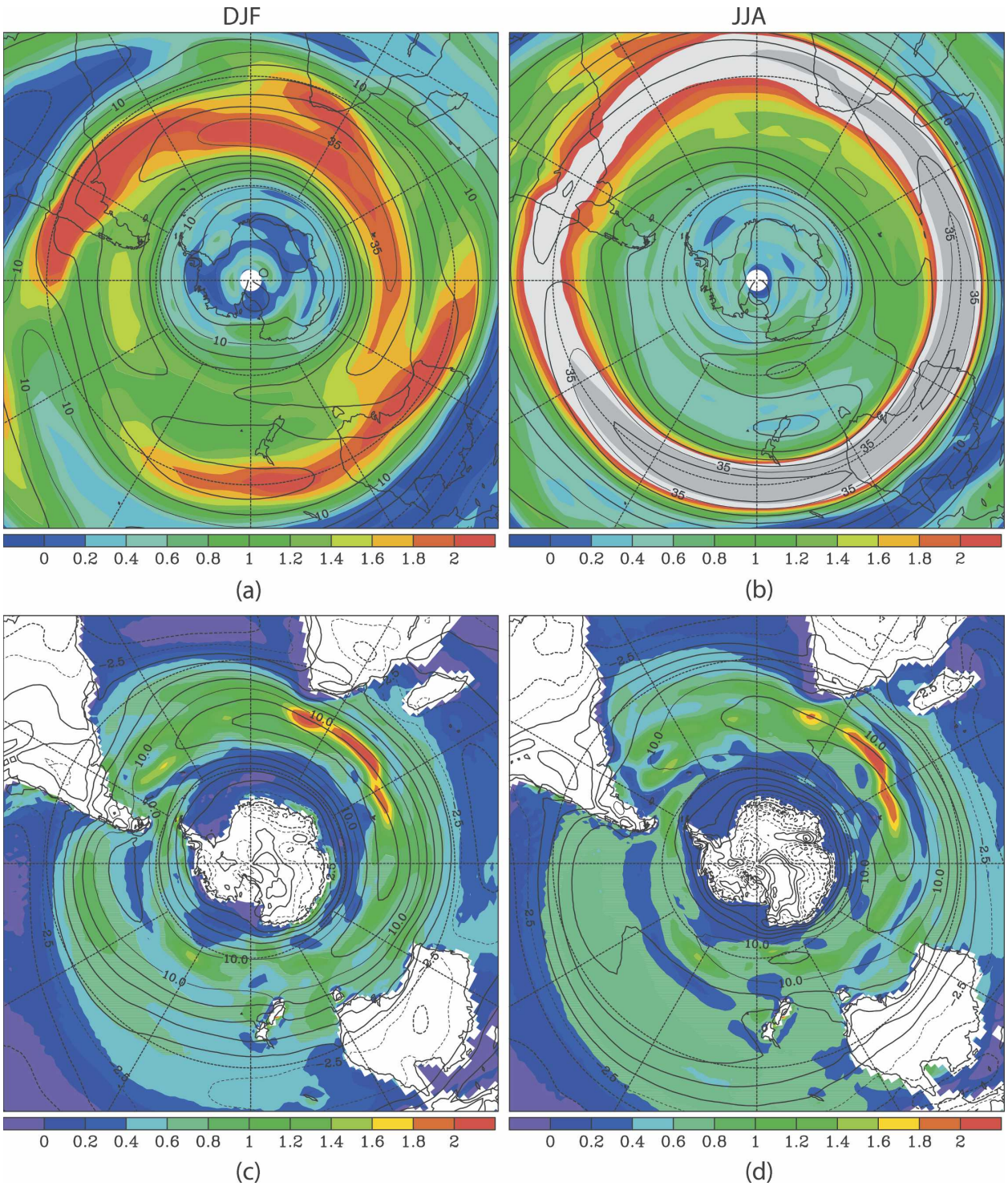

FIG. 1. Mean flow in the upper and lower troposphere for the SH in summer and winter: (a) DJF and (b) JJA pole-to-equator meridional gradient of $\theta_{PV=2}$ (color) in units of K (deg lat)$^{-1}$ and $\overline{U}_{PV=2}$ (contours) with contour interval (c.i.) = 5 m s^{-1}. For $\theta_{PV=2}$, values above 2.2 and 3.0 are represented by two grayscale values. (c) DJF and (d) JJA pole-to-equator meridional gradient of SST (color) in units of K (deg lat)$^{-1}$ and $\overline{U}_{850}$ (contours) with c.i. = 2.5 m s^{-1}.

perature ($\theta_{PV=2}$).[1] For the lower troposphere (Figs. 1c,d), the zonal winds at 850 hPa ($\overline{U}_{850}$) overlaid on the pole-to-equator meridional gradient of SST are shown. In the summer (Figs. 1a,c) the Atlantic and the western Indian Ocean are seen to have generally enhanced meridional gradients in SST and $\theta_{PV=2}$ near 45°S, suggestive of enhanced baroclinic instability there. The zonal winds are strong both near the surface and the tropopause in middle latitudes in the Atlantic and Indian Oceans. In the Pacific, the midlatitude meridional thermal gradients and the zonal winds are generally somewhat weaker. In the winter (Figs. 1b,d), the SST gradients and low-level zonal winds in the Atlantic and Indian Oceans are similar, but the jet is rather less well defined. The major difference from the summer, evident both in the PV = 2 zonal winds and the enhanced meridional θ gradients, is the upper-tropospheric subtropical jet from the central Indian Ocean to the eastern Pacific Ocean. The θ gradient is larger than in the summer around the whole latitudinal circle.

The paper continues in section 2 with a discussion of the ERA-40 dataset and the analysis techniques used. A picture of the storm track as given by Eulerian variances is discussed in section 3. The results of tracking cyclonic systems, and also briefly anticyclonic systems, in winter are given in section 4, and section 5 gives a comparison of tracking results for the four seasons. Some discussion and concluding comments are presented in section 6.

2. Data and techniques

a. Data

The data used in this study are from the ERA-40 (Simmons and Gibson 2000). This has been produced by ECMWF using a modern data assimilation system to combine all the available disparate and inhomogeneous atmospheric observations with a full GCM of the atmosphere. In this way, the most complete four-dimensional view of the atmosphere is produced over the 40+ yr period from 1958 onward (in fact the period covers 1958–2002, a period of 45 yr). ERA-40 uses a three-dimensional variational (3DVAR) scheme for the assimilation of surface, upper air, and satellite observations. The majority of satellite data, Television Infrared Observation Satellite (TIROS) Operational Vertical Sounder (TOVS), Special Sensor Microwave Imager (SSM/I), and cloud motion winds, are available from 1979 onward with increasing amounts of satellite data being used in later periods. Some Vertical Temperature Profile Radiometer (VTPR) data for the period 1972–79 have also been used. The assimilation of satellite radiance data for temperature and humidity is predominately performed by the direct assimilation of the radiances as opposed to the assimilation of variables retrieved from the radiances, which was the usual approach in previous reanalyses. The SSM/I precipitable water content data are assimilated from a 1DVAR retrieval. The model used for the ERA-40 uses a spectral semi-Lagrangian approach for the dynamics with a spectral resolution in the horizontal of triangular truncation 159 (T159) and 60 levels in the vertical. A fully comprehensive physics package is used, including the Rapid Radiation Transfer Model (RRTM) scheme (Mlawer et al. 1997) for the longwave and the scheme of Fouquart and Bonnel (1980) for the shortwave. The influence of subgrid-scale orographic processes is parameterized using the scheme of Lott and Miller (1997), and convection is parameterized using the mass flux scheme of Tiedtke (1989). Full details of the model can be obtained from the Integrated Forecast System (IFS) documentation (White 2000).

In this paper, we discuss diagnostics derived from the whole ERA-40 period. This has the advantage of giving more data to provide significant and stable results. However, it is recognized that some care is required in using such long reanalyses, particularly in the SH, due to changes with time in the types of available observations and their distribution. This is particularly the case with the satellite data, which are sparse before the late 1970s but become the dominant available observation type in the SH after this time. Before the widespread availability of satellite data, the SH was a relatively poorly observed region, with the result that reanalyses in the SH are more dependent on the assimilating GCM for this earlier period. This is a problem when considering trends, and ERA-40 is no different from other reanalyses in this respect (Bengtsson et al. 2004). In terms of the study reported here, an extensive comparison has been made between results based on the full, earlier, and later periods and with other reanalyses. A summary of the sensitivity of the ERA-40 data to the changes in the observing system in the SH and its impact on weather systems diagnostics is given in the appendix. Although there are differences in the number of systems and their intensities between the earlier and later periods, this does not greatly impact the results or modify any of the conclusions reported here. There are also differences in the representation of weather systems between different reanalyses that use different GCMs and different assimilation methodologies This is particularly the case in the SH (Hodges et al. 2003,

[1] It should be noted that θ on PV=2 would increase without bound as the equator is approached. Consequently the field in the Tropics is capped at the value of 380 K.

2004). An indication of this sensitivity is also given in the appendix. However, investigation again suggests that the structures commented on in this paper would be similar if, for example, NCEP reanalysis data had been used and that the conclusions drawn here would not change.

For the seasonal analysis, the usual NH seasonal periods are chosen (DJF, MAM, JJA, and SON). However, there are two particular aspects that complicate the division of the SH year into meteorological seasons. First, as discussed by Hurrell et al. (1998), the average lag in the temperature response (about 44 days) is greater than that in the NH (about 33 days). Second, and more importantly, the SH has a strong semiannual oscillation, in particular in the latitude and strength of the circumpolar surface pressure trough (van Loon 1967). For this paper, these complexities will be ignored and explored further in a future publication.

b. Analysis techniques

The study reported here follows closely a previous one of the NH storm tracks by Hoskins and Hodges (2002). This study explored a wide range of fields for storm-track activity, from the traditional mean sea level pressure (MSLP) to a range of other fields on multiple pressure levels and on potential vorticity and potential temperature surfaces. The use of a wide range of fields allows a contrast to be made between features of different scale. For example, MSLP and geopotential tend to focus on the large-scale end of the synoptic range in a geostrophic sense, whilst vorticity focuses on the small-scale end of the range. Both the Eulerian and system-centered approaches were used to produce storm-track diagnostics. In this paper, a similar approach is taken. Eulerian storm-track diagnostics are produced by identifying the variance in the 2–6-day band based on the Fourier periodogram approach. The filtered variance fields shown here are truncated at total wavenumber 42 and are displayed as standard deviations. The Eulerian variance diagnostics are contrasted with those from a system-centered analysis based on identifying cyclonic or anticyclonic systems, tracking them, and producing statistical distributions from the track ensembles. This has the benefit of being able to separate the cyclonic and anticyclonic activity and determine their differing tracks and attributes.

The tracking is performed using the system of Hodges (1995, 1999). This performs the tracking on the unit sphere. The statistics are also computed on the unit sphere using spherical kernel methods (Hodges 1996) and then scaled to suitable quantities. The fact that the analysis is predominately conducted on the sphere excludes many of the biases that can be introduced when using projections. For the statistics, systems are required to last at least 2 days and to move at least 10° (geodesic). A wide range of statistics is available, such as densities, track, genesis, and lysis as well as mean attributes, such as intensity, growth/decay rate, speed, and lifetime.

Before the tracking is performed, it is considered to be appropriate, and is for some variables necessary, to first remove a background field. This is done by performing a spherical harmonic decomposition of the chosen field and setting the coefficients for total wavenumbers less than or equal to five to zero. This choice of the cutoff is generally conservative in that most synoptic features are almost untouched by it, for example, in vorticity, but it can have a greater impact for variables that represent larger-scale features, for example, MSLP (Anderson et al. 2003). Both positive and negative extrema can be tracked, and for many variables these are associated with either cyclonic or anticyclonic activity. Fields are also reduced to T42 on a Gaussian grid for the tracking analysis to exclude very small scale structures, which occur in fields such as vorticity, and the spectral coefficients have a tapering filter applied to reduce any Gibbs noise (Hoskins and Sardeshmukh 1984). The Eulerian analysis uses the raw fields.

In general, for the tracking analysis the vorticity is the preferred field because it is less influenced by the large-scale background, it is not an extrapolated field to any large extent at the levels used here (850, 500, and 250 hPa), and smaller-scale features are more easily identified. Vorticity can be a very noisy field, but the preprocessing described above helps to reduce much of the noise.

3. Eulerian variance

To show the full seasonal cycle of the SH storm track, Fig. 2 shows the synoptic time-scale variances (2–6 days) converted to standard deviation for 250-hPa vorticity (ξ_{250}) for the four seasons. Nearly all aspects of this are in agreement with previous studies. The summer storm track (DJF; Fig. 2a) is almost circular but has largest magnitudes in the central and eastern Indian Ocean and a break in the region of South America. In autumn (MAM; Fig. 2b) the maximum is in the same location, but the storm track is more broken east of New Zealand. For winter (JJA; Fig. 2c) the picture has changed considerably. The storm track that was present in summer now occupies only the Atlantic and Indian Oceans, after which it spirals in toward Antarctica. However, large variance is now found also in the region of the winter subtropical jet over Australia. Downstream this weakens but then picks up again in the east Pacific. As commented on by others, for example, Tal-

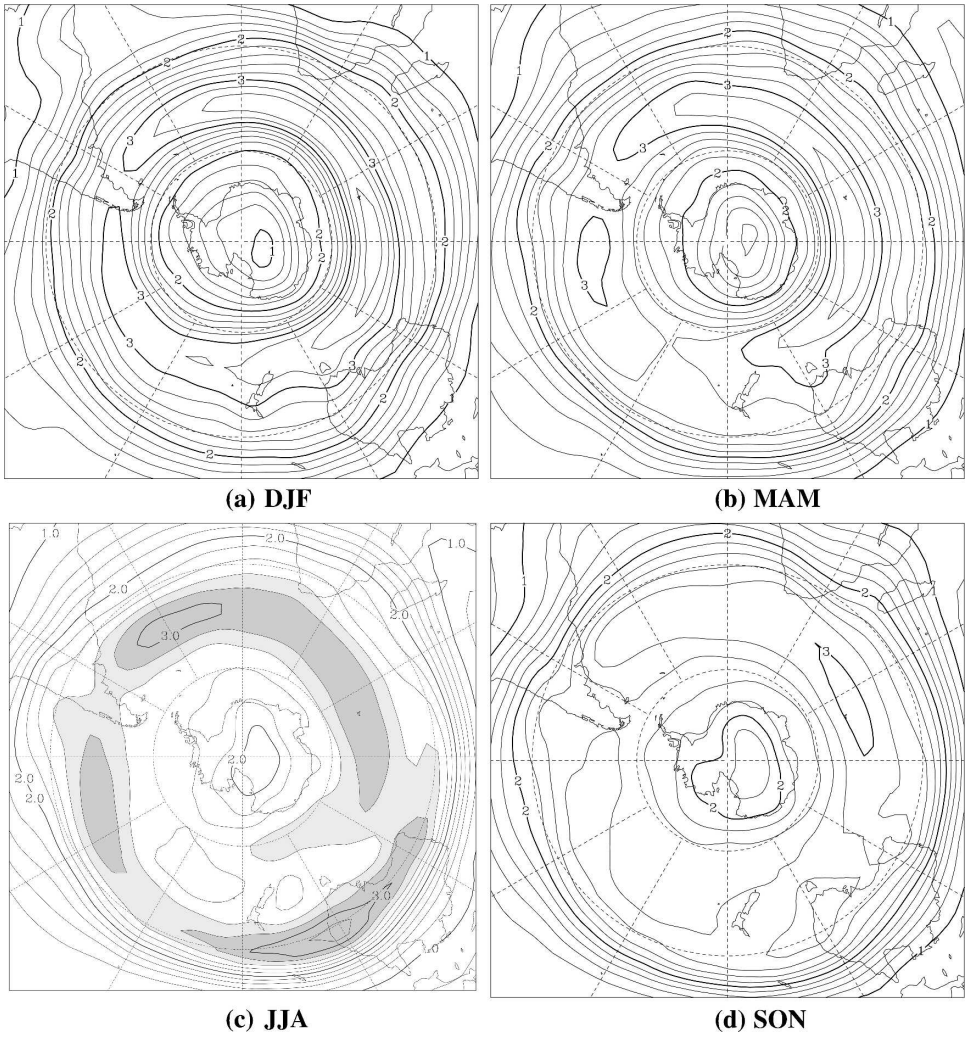

FIG. 2. Bandpass-filtered (2–6 day) variance converted to standard deviation for ξ_{250}: (a) DJF, (b) MAM, and (c) JJA, with shading above 2.6 and 2.8×10^{-5} s^{-1} and (d) SON; c.i. = 0.2×10^{-5} s^{-1}.

jaard (1972), the whole storm track has the appearance of a spiral from Australia, across the Pacific, Atlantic, and Indian Oceans, and in toward Antarctica, with New Zealand sitting between two arms of the spiral. Whereas the autumn picture still has the flavor of the summer picture, spring (SON; Fig. 2d) exhibits a less well defined mixture of winter and summer.

In terms of the absolute maximum values, the strongest ξ_{250} storm track occurs in the summer. The Atlantic/Indian Ocean maxima in summer, autumn, winter, and spring, in units of 10^{-6} s^{-1} are 37, 35, 31, and 31, respectively. However, the winter maximum over eastern Australia is the largest for that season with a value of 33.

Other upper-tropospheric variables show the same sort of picture, but the relative magnitudes of features at different latitudes change with the variable, for example, the height field accentuates high-latitude variability, whereas $\theta_{\mathrm{PV}=2}$ accentuates subtropical variability.

To give a wider view of the seasonal behavior in the upper and lower troposphere, Fig. 3 shows summer and winter synoptic-scale variance as standard deviations for meridional wind at 250 (V_{250}) and 850 hPa (V_{850}), and for MSLP. The V_{250} (Figs. 3a,b) shows very similar storm tracks and seasonal behavior to those already discussed for ξ_{250} (Figs. 2a,c). The upper-tropospheric behavior can be compared with that at 850 hPa (Figs. 3c,d). The summer circumpolar loop here is not totally lost in the winter, there being little sign of the spiral toward Antarctica, no Australian maximum, and a significant Pacific storm track. The summer, autumn, winter, and spring V_{850} standard deviation maxima are 5.4, 6.7, 6.1, and 6.0 m s^{-1}, respectively. In contrast to the

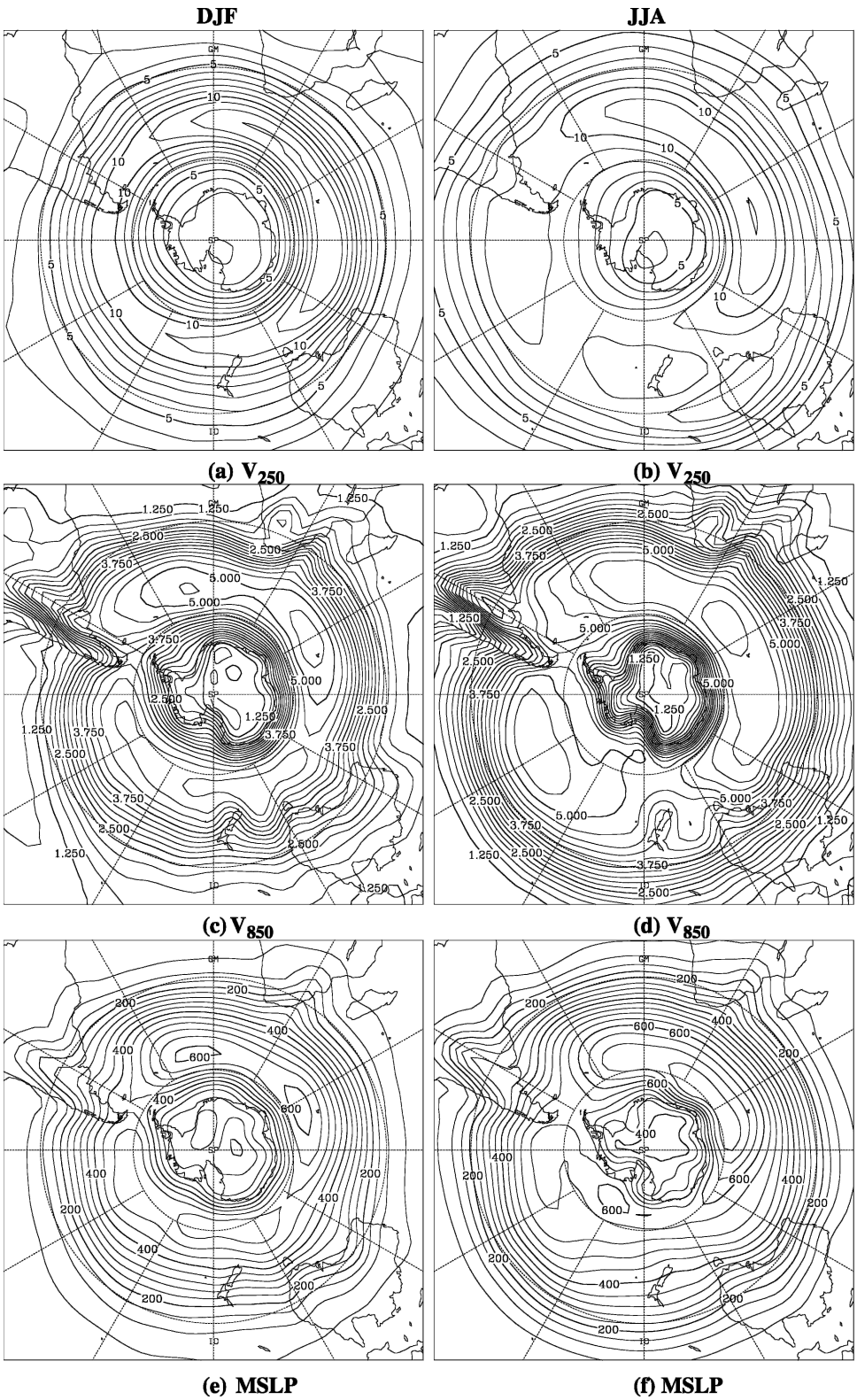

FIG. 3. Bandpass-filtered (2–6 day) variance converted to standard deviation for (a) DJF, V_{250}, c.i. = 1 m s^{-1}; (b) JJA, V_{250}, c.i. = 1 m s^{-1}; (c) DJF, V_{850}, c.i. = 0.25 m s^{-1}; (d) JJA, V_{850}, c.i. = 0.25 m s^{-1}; (e) DJF, MSLP, c.i. = 50 Pa; and (f) JJA, MSLP, c.i. = 50 Pa.

upper troposphere, here summer is the weakest and autumn is the strongest. The main storm tracks in the lower troposphere coincide well with, but are a few degrees poleward of, the upper-tropospheric storm tracks.

Like the height field in both the upper and lower troposphere, MSLP (Figs. 3e,f) accentuates the high-latitude behavior, showing in all seasons a high-latitude storm track in the Atlantic and Indian Oceans with a spiral southward toward the Ross Sea region (160°W) in the winter. In contrast to $V_{850,}$ for MSLP the maximum values are largest in winter, slightly reduced in the transition seasons, and smallest in summer. The storm track shifts slightly in latitude with the seasons, being closest to the pole in winter. A separate east Pacific storm track is evident in winter only, though not as clear as it is in V_{850}. The winter and summer storm tracks as shown by the variance in V_{850} are nearly collocated with the maximum SST gradients shown in Figs. 1c,d. However, this is not the case for that delineated by MSLP.

4. Winter storm tracking

In this section, the focus is on the winter (JJA), the season with the most enhanced zonally asymmetric, spiral storm track. A summary of some of the results of tracking cyclonic features in the upper and lower troposphere is given in Fig. 4, in which track densities (colors) and average system intensities (line contours) are shown. To represent the upper troposphere, the variables used here are ξ_{250} and $\theta_{PV=2}$. The track density for ξ_{250} (Fig. 4a) shows a loop, at most longitudes, around the pole and an outer subtropical track covering about 180° of longitude in the sector of the strong subtropical jet. In the eastern Pacific/western Atlantic, there is an indication of a spiral linkage between the two regions. This behavior is similar to that suggested by the variance of this field (Fig. 2c). The $\theta_{PV=2}$ field has its largest variance in the subtropics, and consequently the track density of cyclonic (cold) features in this field (Fig. 4b) emphasizes the subtropical track and indicates fewer high-latitude tracks in the Indian Ocean and Ross Sea regions. The average intensities of the systems for ξ_{250} are largest on the equatorward side of the subtropical track, in the range 7.5–11 $\times 10^{-5}$ s^{-1}, and drop to 5–6 $\times 10^{-5}$ s^{-1} on the high-latitude side. The intensities for $\theta_{PV=2}$ generally behave in a similar manner. However, in the east Pacific, whereas the $\theta_{PV=2}$ track density and intensity both highlight the subtropical jet region, for ξ_{250} this is true for the intensity but, as already discussed, not for the track density, which marks the start of the poleward spiral.

The lower-tropospheric behavior is indicated by results for ξ_{850} and MSLP in Figs. 4c and 4d, respectively. The ξ_{850} track density emphasizes the primary spiral storm track from the Atlantic and Indian Oceans and then around Antarctica to the Antarctic Peninsula (60°W). The average intensities of systems is largest here, generally 5 to 6 $\times 10^{-5}$ s^{-1}. The upstream end of this track, to the east of South America, shows intensity maxima at low and high latitudes and a density maximum in between. This will be discussed further below. The MSLP (Fig. 4d) shows a high-latitude track with large track density and with mean intensity values being generally in the range of 20–27 hPa, but again there are hints of interesting behavior near South America. Both fields indicate large track density near Antarctica upstream of the Ross Sea and large intensities downstream of this; ξ_{850} also shows an intensity maximum and a weak density maximum near 40°S, indicating the Pacific storm track, and lower storm incidence and intensity eastward from Tasmania through the southern island of New Zealand, a major blocking region (e.g., Trenberth and Mo 1985).

From Figs. 4a,c it is clear that the main storm track spiraling from South America to the Antarctic Peninsula is coupled through the depth. The subtropical jet cyclonic disturbances are upper level only in the Indian Ocean, but there is coupling through the depth again in the Pacific as the tracks spiral poleward to South America. Upstream of South America at 250 hPa, there is a clear distinction between the track density maximum, which is the extension of the deep systems, and some 15° equatorward of it the intensity maximum, which indicates strong, shallow systems on the subtropical jet. Eulerian variance statistics give little indication of this behavior. However, Vera et al. (2001) using extended empirical orthogonal functions (EOFs) applied to the 300-hPa meridional wind in the South America region did identify subtropical synoptic-scale waves as well as the more usually identified midlatitude waves. They also found the subtropical waves to have less signature at 850 hPa upstream of the Andes.

Further diagnostics of the cyclonic ξ_{850} wintertime systems are presented in Figs. 5a–d. Figure 5a shows the average speed of the cyclonic weather systems (contour lines) and their mean lifetimes (colors). The average speeds and directions (not shown) reflect the mean flow at about 700 hPa, with a maximum average speed in the western Indian Ocean of about 18 m s^{-1} and closer to 14 m s^{-1} elsewhere. The direction of movement is predominantly eastward, with a small poleward component that is much enhanced in the eastern Indian Ocean extending through to the western Pacific, consistent with the spiral track picture there. The average lifetime of systems is remarkably uniform at 5–6 days but is lower around Antarctica (~4 days) and higher in the

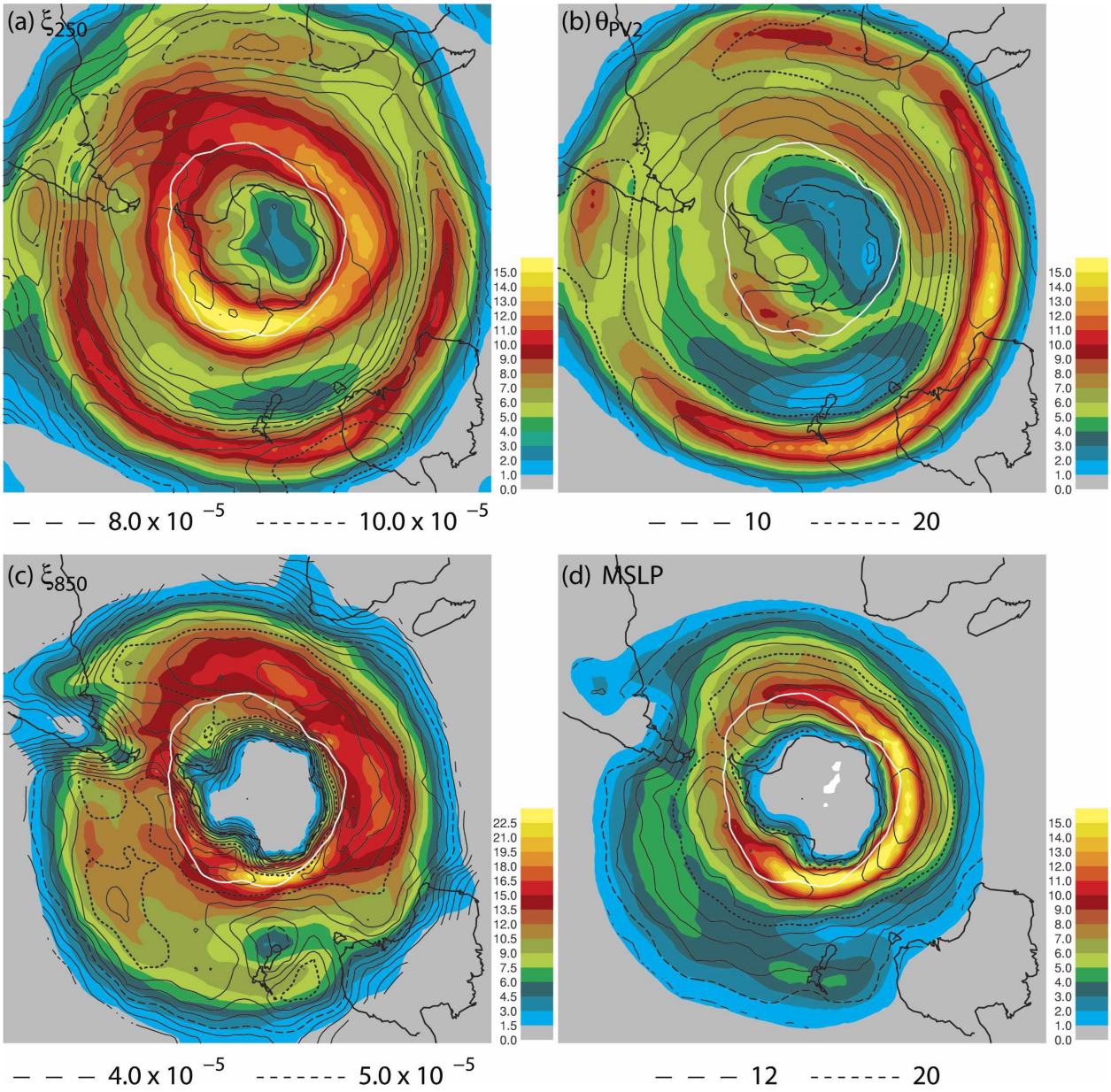

FIG. 4. Winter (JJA) cyclonic track density (color) and mean intensity (line contour) using (a) $\xi_{250,}$ c.i. = 0.5×10^{-5} s^{-1}; (b) $\theta_{PV=2}$, c.i. = 2 K; (c) $\xi_{850,}$ c.i. = 0.25×10^{-5} s^{-1}; and (d) MSLP, c.i. = 2 hPa. Track densities are in units of number density per month per unit area where unit area is equivalent to 5° radius spherical cap; intensities are absolute relative to the removed background. The 50% sea ice boundary is delineated by the white line.

subtropical western Pacific (~7 days). However, this distribution is somewhat biased by the fact that only mobile systems that live longer than 2 days contribute to the statistics.

The average ξ_{850} cyclonic growth/decay rates, genesis, and lysis results in Figs. 5b, 5c, and 5d, respectively, are conveniently discussed together. Overall there tends to be genesis and growth at low latitudes and decay and lysis at high latitudes near Antarctica. However, the behavior is much richer than this. The genesis region on the eastern side of Australia is followed downstream by another genesis maximum centered over the north island of New Zealand. There is growth down to 40°S in the central Pacific and genesis there and in the eastern Pacific. There is large decay where the deep Pacific storm track meets the upslope side of the Andes, and downstream there is large growth. Corresponding to this, near 45°S, there is lysis upstream

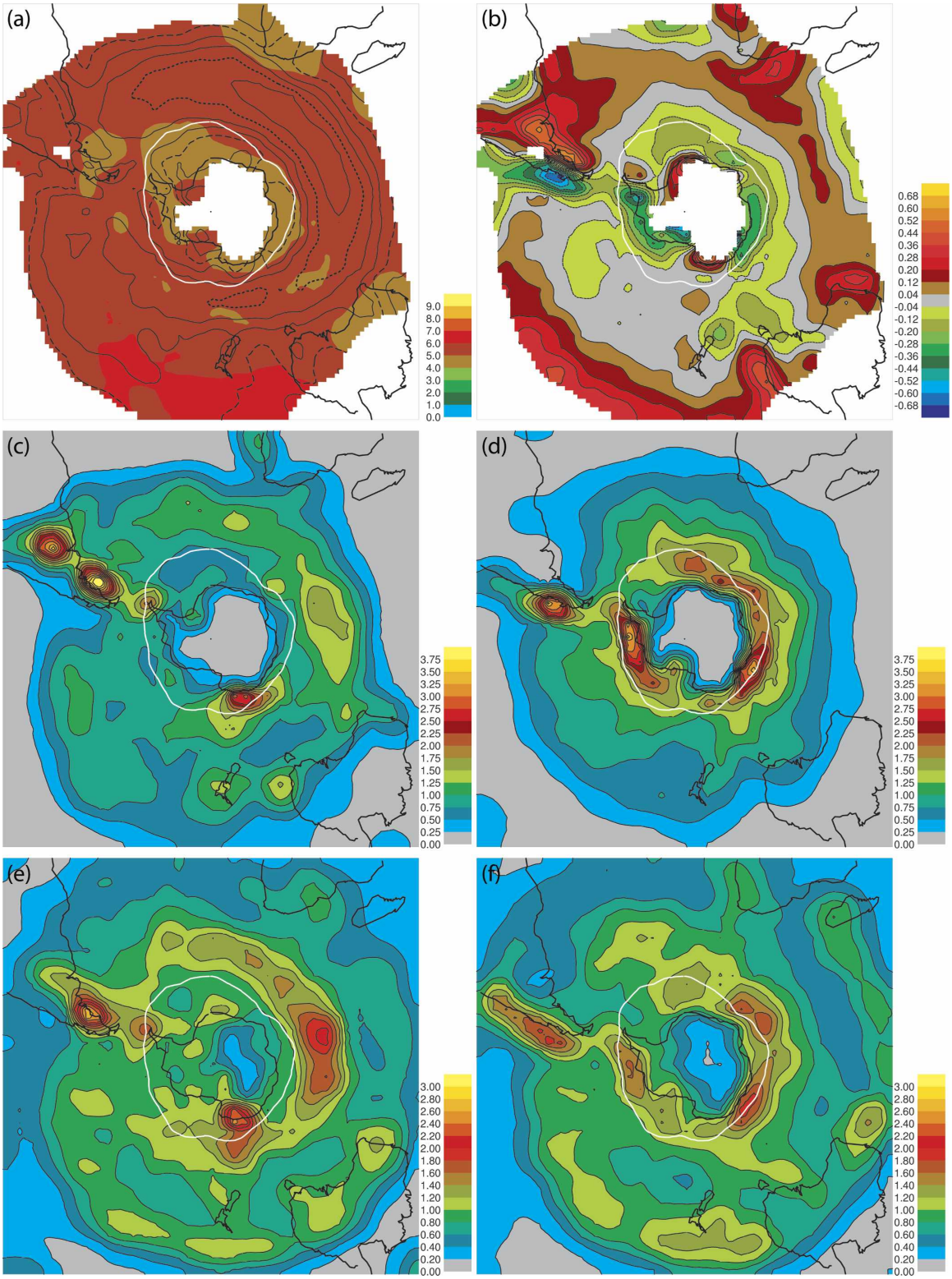

FIG. 5. Winter (JJA) cyclonic statistics for (a) ξ_{850} mean lifetime (color; unit is days) and mean speed (line contour; c.i. = 2 m s^{-1}), where dashed line is 10.0 m s^{-1} and dotted line is 16 m s^{-1}; (b) ξ_{850} mean growth/decay rate (unit is day^{-1}); (c) ξ_{850} genesis density; (d) ξ_{850} lysis density; (e) ξ_{500} genesis density; and (f) ξ_{500} lysis density. Density units are number density per month per unit area with the unit area as in Fig. 4. The 50% sea ice boundary is delineated by the white line.

and genesis downstream. The genesis is rather larger than the lysis, which means that it is not simply that the 850-hPa systems disappear only to reappear on the downstream side of the Andes.

Farther north, near 30°S, there is another concentrated genesis and growth region with no corresponding upstream lysis. This is where the strong, shallow systems on the subtropical jet, indicated in Fig. 4a, cross the high Andes, and it seems likely that the leeside genesis is associated with these.

Continuing the discussion of Figs. 5b–d, there is growth and genesis across the Atlantic and Indian Oceans, with maxima to the south of South Africa and in the central Indian Ocean. Associated with both western and eastern South Africa, there is also growth and genesis, in agreement with the surprising sensitivity of the storm track to the presence of South African topography found in the numerical experiments of Inatsu and Hoskins (2004). There is quite localized lysis and decay near Antarctica between 90° and 135°E followed, between 135°E and 180°, by the major genesis and growth region at these high latitudes. This is consistent with the storm-track density maximum downstream of this commented on above and seen in Figs. 4c,d. At the eastern end of this, there is decay and lysis, particularly upstream of the Antarctic Peninsula. In the lee of this and also in the Weddell Sea, there is the second, weaker high-latitude region of growth followed by lysis. Along with the two genesis maxima over South America, the Antarctic Peninsula gives a third genesis region upstream of the Atlantic storm track.

Whilst the SST gradients shown in Fig. 1 would suggest strong baroclinicity in the Atlantic and Indian Ocean regions and hence strong growth, the mean growth/decay statistic (Fig. 5b) shows relatively weak growth in this region. However, this is just an artifact of the averaging together of similar numbers of growing and decaying systems (see later discussion). In fact separating the growth from the decay and regenerating the statistic (not shown) indicates that for growing systems the mean growth through the Atlantic and Indian Oceans is $\sim$0.5 day^{-1} whilst the mean decay is $\sim$0.4 day^{-1}. This also occurs in other regions, for example, the Pacific has $\sim$0.35 day^{-1} for both growth and decay, although for the major genesis or lysis regions associated with the Andes there is predominately growth or decay, respectively.

To exhibit information on vertical structures in general and in particular in the region of the Andes, genesis and lysis of 500-hPa cyclonic vorticity features (ξ_{500}) are presented in Figs. 5e and 5f, respectively. It is clear that the genesis in the Atlantic and Indian Ocean regions and lysis near Antarctica are deep. Activity also reaches down to this level from the upper-tropospheric subtropical jet. Focusing on the South American region, it is worth noting that, unlike the 850-hPa level, this surface is above ground almost everywhere so that any lysis and subsequent genesis across the Andes cannot be attributed to the disappearance of the surface. Where the main storm track intercepts the Andes, as at 850 hPa, there is lysis on the upslope and larger genesis on the downslope. Where the subtropical jet moves over the Andes, there is much larger lysis at 500 hPa than at the lower level. In contrast, the genesis is much weaker than at 850 hPa and somewhat weaker than the upstream lysis. These properties are strongly supportive of the hypothesis that it is the middle- and upper-tropospheric cyclonic features on the subtropical jet impinging on the Andes that lead to the generation of lower-tropospheric cyclones in its lee.

To test this hypothesis, each of the 850-hPa genesis events in this region was investigated to determine whether there was a preexisting feature at 500 hPa that passed within 500 km, with at least 10% of the points on the two tracks overlapping in time. Most 500-hPa cyclonic systems do not cause such genesis. However, for 75% of the lower-tropospheric genesis events in this region such a preexisting and contemporaneous midtropospheric cyclonic feature could be identified, and for 61% it was to the west of the lower system. The criteria for association used here are quite strict, and it is probable that nearly all the low-level genesis events are in fact associated with preexisting mid- or upper-tropospheric waves. Berbery and Barros (2002) have discussed the transport of moisture from the Tropics into the La Plata River basin (east of the Andes and approximately between 15° and 38°S) by the low-level northerly jet on the eastern side of the Andes. They found that this moisture transport is a maximum in winter and spring. Latent heat release fueled by the low-level jet could be important in the low-level subtropical cyclogenesis process. It is notable that in the North American winter, (Hoskins and Hodges 2002, their Fig. 6c) similar separate high-latitude and subtropical jet location genesis maxima were also found in the lee of the Rockies.

Because many of the ξ_{850} cyclone genesis regions are so well defined, it is of interest to consider the fate of all the systems that are generated in these regions. This can be done by isolating all those systems that are initiated in a genesis region and reconstructing the statistics for these systems alone. To do this, a 5° radius spherical cap sampling region is centered over each genesis region (this can also be done for lysis). An example of this is shown in Fig. 6a for all the winter tracks in ERA-40 that originated in the cyclogenesis region

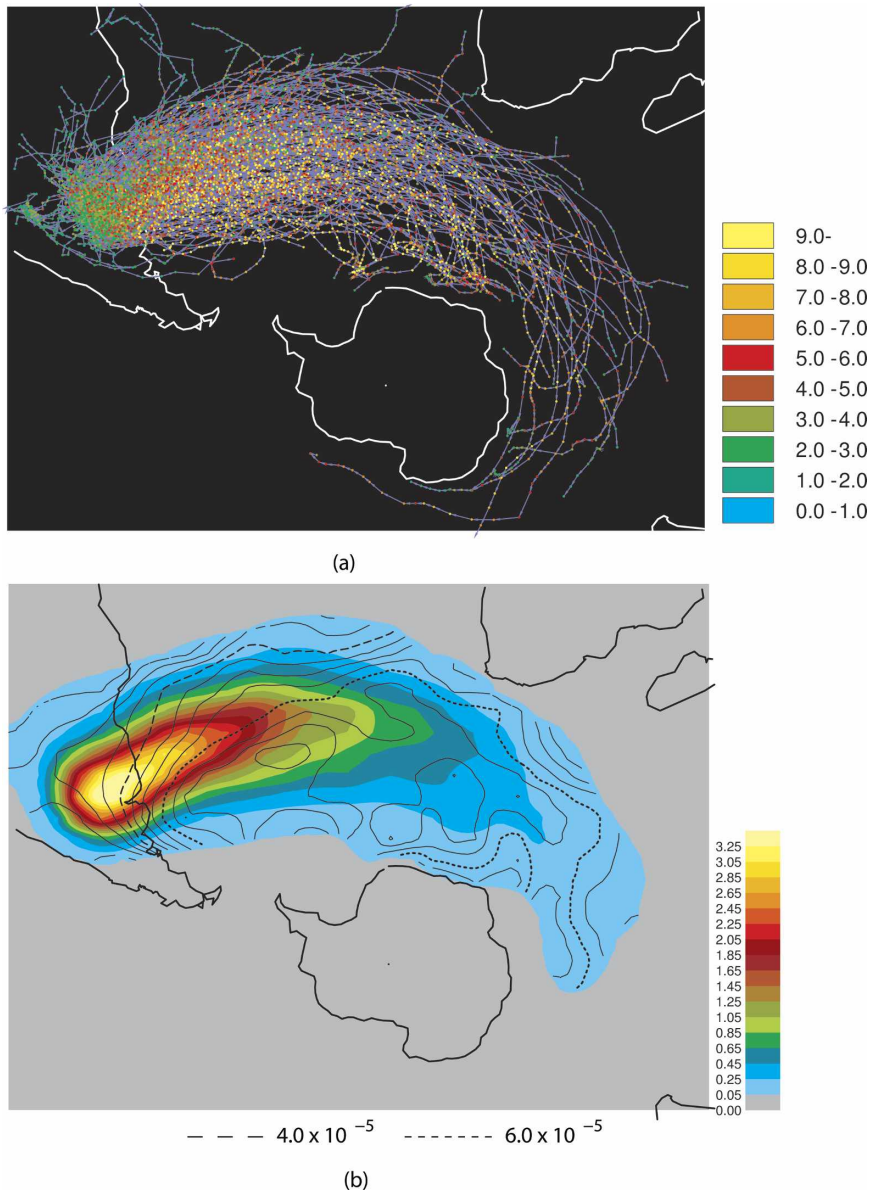

FIG. 6. (a) Trajectories of all cyclonic systems identified in ξ_{850} originating in the cyclogenesis region near 30°S over South America. Colored points indicate intensity at each 6-hourly time step in units of 10^{-5} s^{-1}. (b) Track density (color) and mean intensity (line contours) for the same systems. Track density has the same units as in Fig. 4, and mean intensity c.i. = 0.5 $\times$ 10^{-5}, relative to removed background.

near 30°S over South America. The dots show the position and their color the intensity of each system every 6 h. The compactness of the distribution is remarkable for a 45-yr period. To help interpret this picture, Fig. 6b shows the track density and mean intensity distributions. The average speed and lifetimes of systems given previously suggest an average track of some 90° in longitude. This accords well with what is seen here. Many travel less than this, and some travel considerably farther with the one system almost making a full circuit. The amplitudes generally increase as the cyclones move downstream and poleward, with an indication that the stronger systems have larger poleward movement.

To provide an extension of this picture that gives a view of the whole winter lower-tropospheric storm track, a similar set of statistics has been generated for most of the genesis regions picked out when discussing Fig. 5c, although to produce the track density shown in

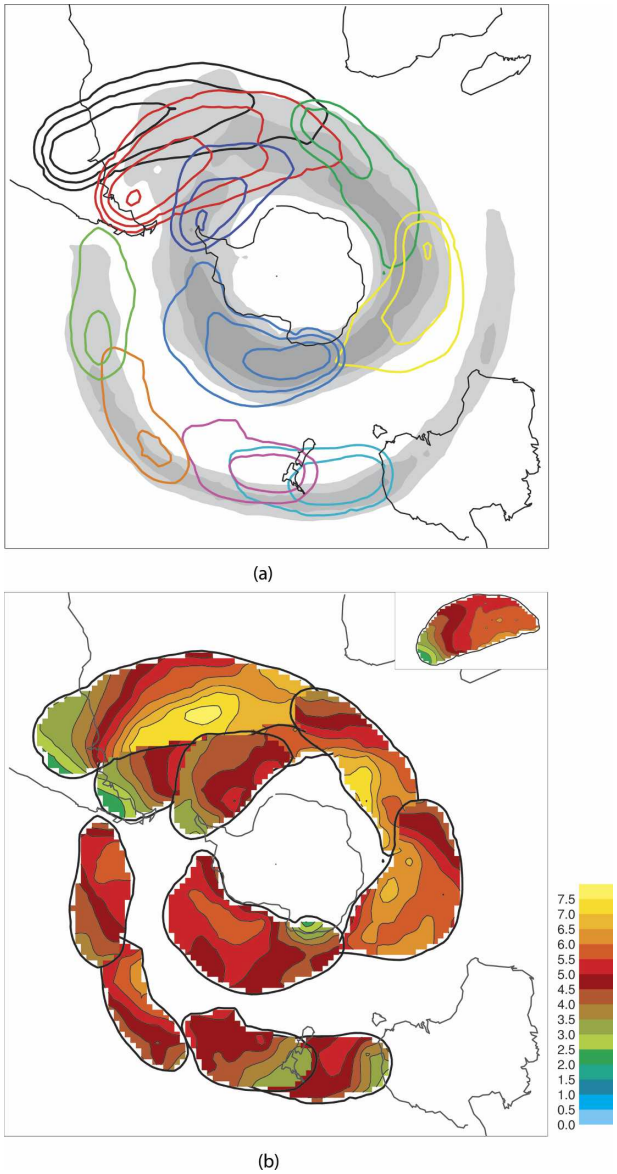

FIG. 7. Statistics for the main ξ_{850} genesis regions. (a) Rubber band track density contours; levels at 0.5, 1.0, 2.0, and 4.0 in units of number density per month per unit area with unit area as in Fig. 4; the grayscale background indicates the track density in ξ_{250} for values above 9.0 (see Fig. 4a). (b) Mean intensities restricted to within the 0.5 track density contour, in units of 10^{-5} s^{-1}. Inset is for the Antarctic Peninsula genesis masked by the South America genesis plots in the main plot.

Fig. 4c requires genesis that occurs throughout the storm track. The results for the track densities and intensities are summarized in the overlapping plate storm-track diagrams shown in Figs. 7a and 7b, respectively. The two genesis regions of South American and the genesis of the Antarctic Peninsula provide cyclones that feed the Atlantic track; the genesis maximum off South Africa feeds the Indian Ocean track; the Indian Ocean genesis feeds the spiral toward Antarctica; the genesis upstream of the Ross Sea feeds the track toward the Antarctic Peninsula. Equatorward of this, the east Australian and New Zealand genesis regions feed the Pacific track, and genesis there feeds systems into the southern South American lysis and genesis region. The intensity picture shows the expected generality of larger amplitudes downstream and poleward. It also emphasizes the importance of the equatorward generation region over South America and of the genesis regions in the Atlantic and Indian Oceans. Each of the panels in Fig. 7 emphasizes typical life cycles of lower-tropospheric cyclonic features. However, the whole overlapping plate picture depends on, and is consistent with, the downstream propagation and development of synoptic wave activity in the upper troposphere (Simmons and Hoskins 1979; Berbery and Vera 1996; Chang 1999; Rao et al. 2002). To show this relationship, large values of the track density of upper-tropospheric cyclonic features are indicated in grayscale in Fig. 7a. The upper-tropospheric link is seen in its spiral from Australia around the hemisphere and back to the coast of Antarctica, with lower-tropospheric development occurring in favorable regions or at the end of the previous life cycle.

Given the research done on cyclones near Antarctica, it is of interest to isolate systems that grow or decay there. A summary of the tracks from cyclogenesis and cyclolysis that occur around the Antarctic coast is obtained by using a circular sampling region around Antarctica of radius 27.5° centered on (87.5°S, 80°E). The track density and mean intensities for these systems are given in Fig. 8. Systems that are generated near Antarctica are generally found to remain near it (Fig. 8a). The region of most tracks stretches from the Australian sector to the Antarctic Peninsula, and there is a weak intensity maximum in the Ross Sea sector. However, there is a secondary region in both track density and intensity associated with the genesis in the Wedell Sea commented on previously. The lysis (Fig. 8b) shows that whilst much of the activity close to the coast originates there, there is also a significant proportion that originates from lower latitudes. The intensities are generally high but decrease toward the coast. It should be noted however that only long-lasting, mobile systems have been considered here; much more cyclogenesis occurs around the Antarctic coast that is mesoscale and shorter lived and often semistationary. In particular, cyclones generated in the embayments often do not become very mobile, though clearly some do, as seen in the Weddell Sea.

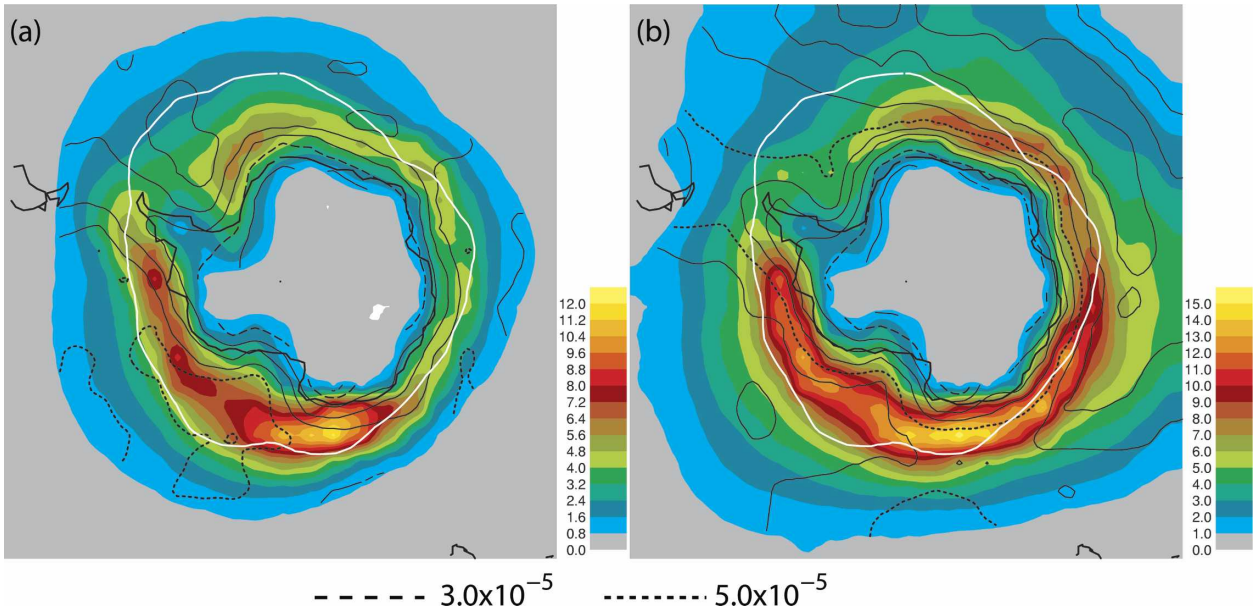

FIG. 8. Track density and mean intensities around Antarctica based on ξ_{850} for (a) cyclogenesis that occurs around Antarctica and (b) cyclolysis that occurs around Antarctica. Track density is number density per month per unit area (unit area as in Fig. 4), and mean intensity is absolute relative to removed background with c.i. = 0.5×10^{-5}. The sampling region for selecting tracks is defined by a spherical cap of radius of 27.5° centered on 87.5°S, 80°E; the 50% sea ice boundary is delineated by the white line.

Since the SH storm track does not only consist of migratory cyclones but also mobile anticyclones, it is also of interest to consider their contribution. Figure 9 summarizes some of this behavior in winter. There is generally a single 250-hPa latitudinal maximum in the density and intensity of anticyclonic vorticity features (Fig. 9a), located near 55°S, between the high-latitude and subtropical cyclonic tracks (Fig. 4a). The mobile anticyclone track density and intensity are both weakest in the Atlantic and strongest in the Australian/New Zealand sector. In the east Pacific, there is also an intensity maximum near 45°S associated with the Pacific storm track. The ξ_{850} track density and intensity (Fig. 9b) also gives a circumpolar loop picture. There is enhanced activity south of New Zealand, but there are also similarities with the results for the cyclonic features (Fig. 4c) with activity downstream from South America, across the Atlantic and Indian Oceans, and in the Pacific signs of both middle- and high-latitude activity. Diagnostics for MSLP (not shown) also show the circumpolar behavior but with track density and intensity maxima in the western Indian Ocean and the largest intensity maximum in the eastern Pacific near 60°S.

Figure 9c gives the genesis of ξ_{850} anticyclonic features. There is an anticyclogenesis maximum over southern New Zealand that is present in all seasons, with largest values in the summer and autumn. However, the most striking aspect is perhaps the two maxima in anticyclogenesis over South America that are located in latitudes poleward of the two cyclogenesis regions there (Fig. 5c). There is also one poleward of the cyclogenesis region over the Antarctic Peninsula. Intriguingly, the same relative positions of cyclogenesis and anticyclogenesis maxima are found in the lee of the Rockies in the boreal winter. The anticyclonic systems originating in the South America regions, whilst being mobile in the context of our admission criteria, in general travel much shorter distances than the cyclones.

There is often discussion of cyclogenesis in the lee of topography, but anticyclogenesis associated with topography may be less expected. A clearer picture of the behavior in the Andes region at a level above the topography is given by the lysis and genesis of anticyclonic (Figs. 9d,e) and cyclonic (Figs. 9f,g) ξ_{500} features. To resolve the spatial relationships, reduced smoothing and higher resolution was used for the construction of these diagnostics. Proceeding from west to east, there is anticyclolysis upstream, followed by cyclolysis on the upslope, anticyclogenesis over the mountains, and cyclogenesis in the lee. This pattern of events is consistent with the stretching and shrinking of vortex tubes below an isentrope that passes over the topography but which has a broader, shallower shape (see, e.g., Holton 1992). An air column approaching from the west first experiences some stretching, which gives a small cyclonic tendency. This is followed by large shrinking and anticy-

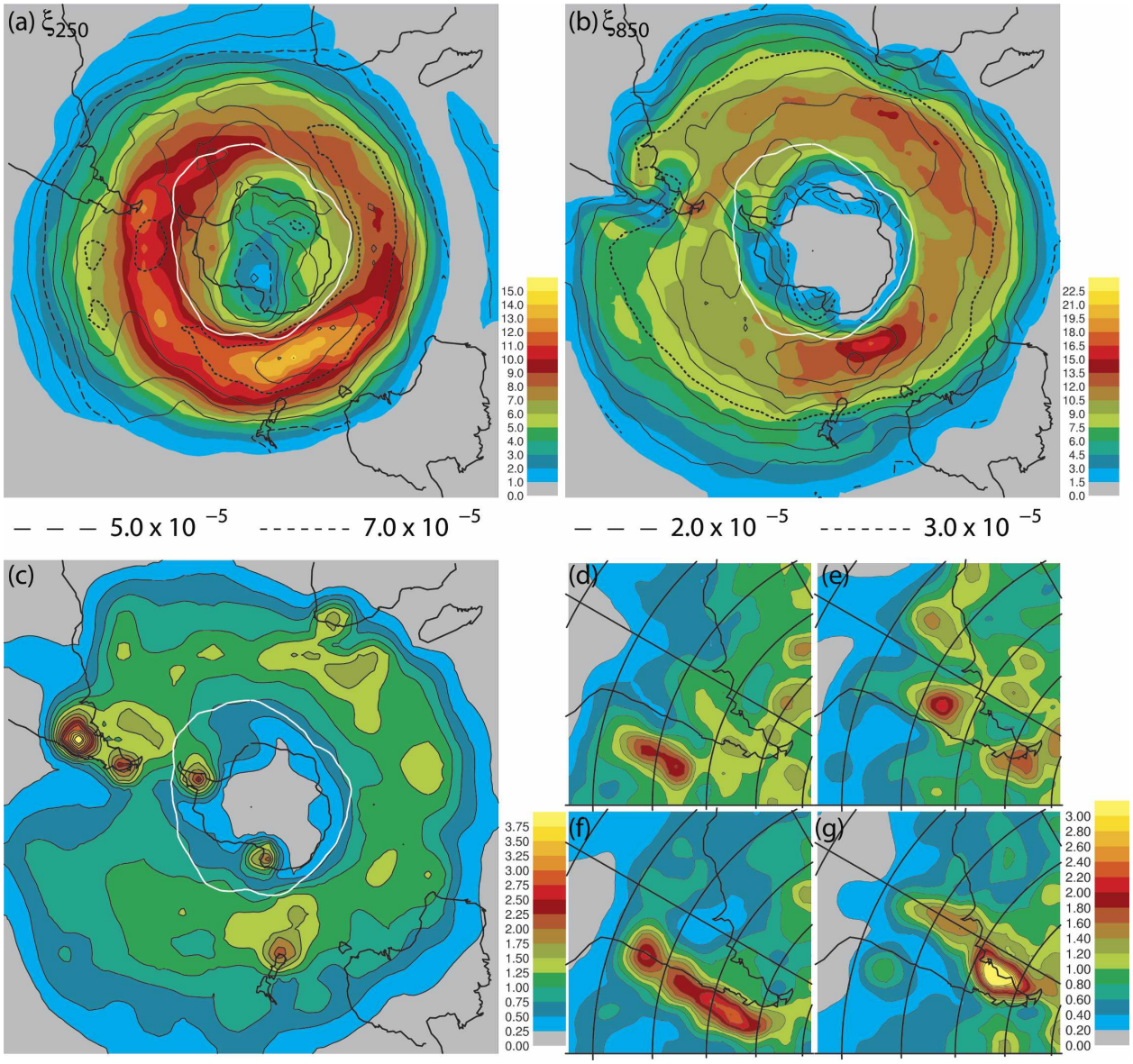

FIG. 9. Winter (JJA) anticyclonic track density (color) and absolute mean intensity (line contour) using (a) ξ_{250}, c.i. = 0.5×10^{-5} s^{-1}; and (b) ξ_{850}, c.i. = 0.25×10^{-5} s^{-1}. (c) The anticyclogenesis density for ξ_{850}. (d)–(g) Lysis and genesis for anticyclones and cyclones in the vicinity of the Andes for ξ_{500}: (d) the anticyclolysis density, (e) the anticyclogenesis density, (f) the cyclolysis density, and (g) the cyclogenesis density. Densities are in units of number density per month per unit area (unit area as in Fig. 4). Intensities are absolute relative to the removed background. The 50% sea ice boundary is delineated by the white line.

clonic tendency, which lasts until the peak of the topography. Farther east there is large stretching and cyclonic tendency.

5. A comparison of tracking results for the seasons

In this section, some results will be presented for the seasonal variation of cyclonic systems as given by tracking diagnosis. Figure 10 shows the track density and mean intensity of cyclonic features for the upper troposphere in ξ_{250}. As was found to be the case using Eulerian variance, the main summer (DJF) storm track (Fig. 10a) is nearly circularly symmetric with maximum system intensities in the Eastern Hemisphere and everywhere on the equatorward edge of the track density maximum. In comparison with the winter picture, which is repeated in Fig. 10c, the summer track is located between the winter subtropical and polar loops,

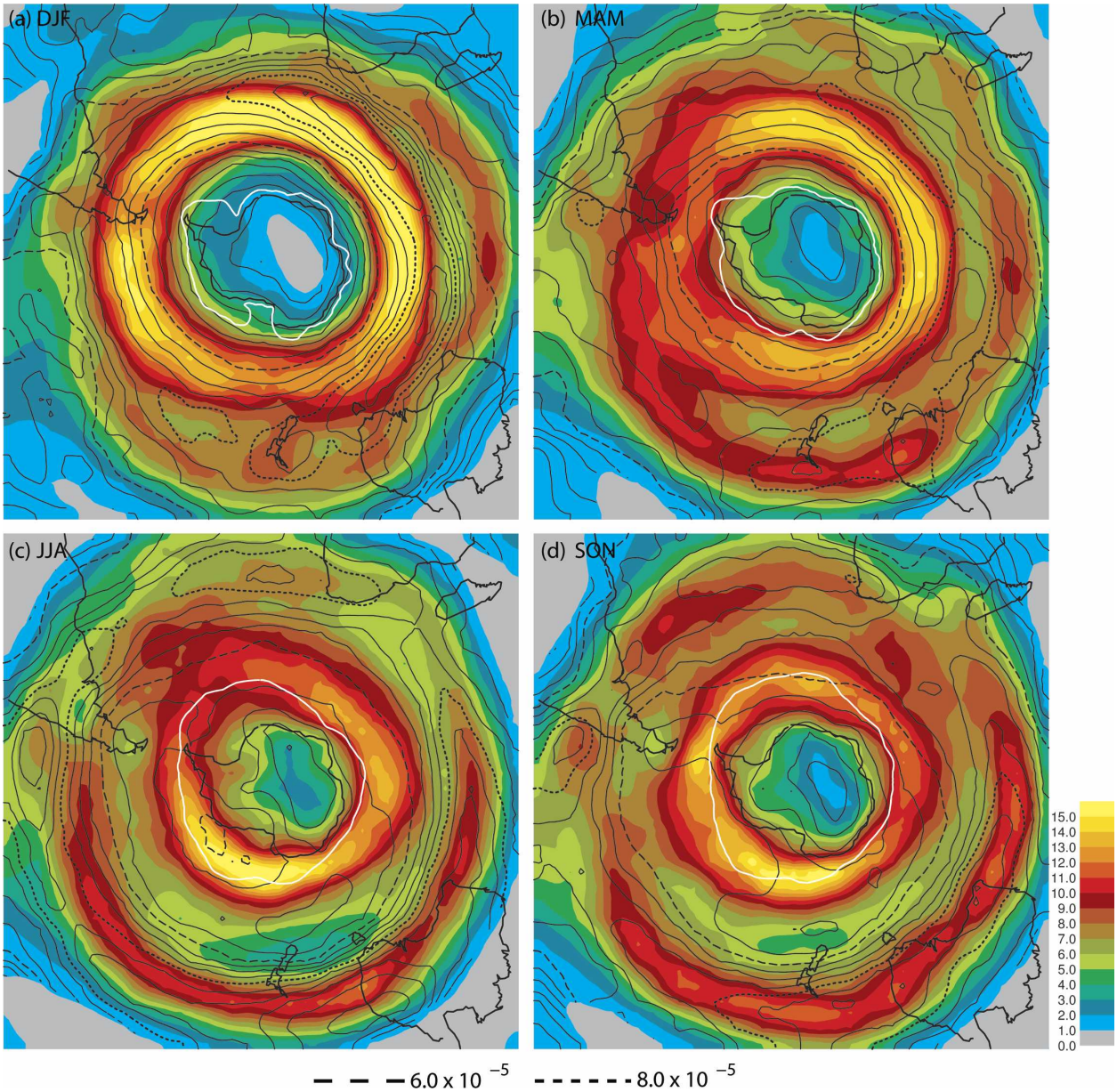

FIG. 10. Upper-tropospheric seasonal cycle of the SH storm track based on ξ_{250}: track density (color) and mean intensity (line contour) for (a) DJF (summer), (b) MAM (autumn), (c) JJA (winter), and (d) SON (spring). Track density is number density per month per unit area (unit area as in Fig. 4), and mean intensity is absolute relative to removed background with c.i. = 0.5×10^{-5}. The 50% sea ice boundary is delineated by the white line for each season.

and the summer intensities are generally greater than those in the winter polar loop but less than those in the subtropical loop. As was the case with Eulerian variance, autumn (MAM; Fig. 10b) is more similar to summer, and spring (SON; Fig. 10d) to winter. However, here autumn already shows the subtropical storm track in the Australian/New Zealand sector, with the two tracks joining in the east Pacific.

In the lower troposphere (Fig. 11), the ξ_{850} tracks have a circumpolar appearance in summer (Fig. 11a) compared with the winter picture of a spiral plus a Pacific track as shown in Fig. 11c. Throughout the year, the largest intensities are found in the Indian Ocean. At this level, this maximum is smallest in summer, and in winter it is slightly larger than in the equinoctial seasons.

Another aspect of the summer ξ_{850} picture is the relatively large track densities found in regions of the sub-

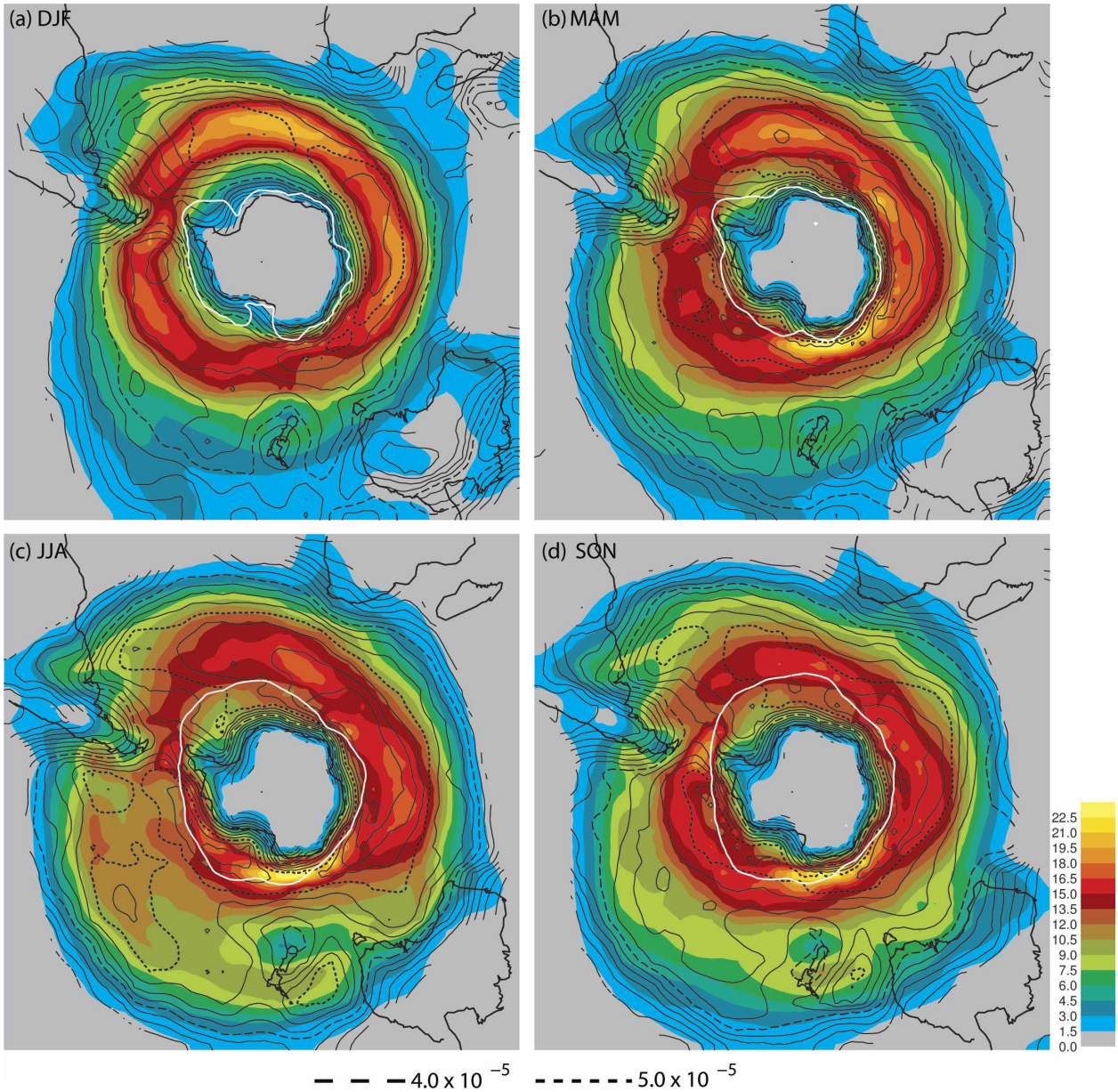

FIG. 11. Same as in Fig. 10, but for lower-tropospheric seasonal cycle based on ξ_{850}. Mean intensity is absolute relative to removed background with c.i. = 0.25×10^{-5}.

tropics, particularly in the western Atlantic and western Pacific Oceans. To look at this and other features further, Fig. 12 shows the summer ξ_{850} cyclogenesis on an expanded latitudinal domain. The zonally elongated genesis regions equatorward of 20°S near 0°, 75°E, 130°E, and 90°W all lead to westward-moving weak tropical systems. Near 60°W there are three genesis regions in the lee of the Andes over South America, near 47° and 32°S, and over the Antarctic Peninsula that correspond closely to the winter genesis regions (Fig. 4c), though all except that at 47°S are weaker. The Andean genesis maxima also have anticyclogenesis maxima in close proximity (not shown) similar to the winter, although these now occur to the southwest of the genesis maxima, with the more southerly one being the most intense. These changes appear to be closely tied to changes in the upper-tropospheric jet over South America as discussed above and the interaction with the flow over the topography and clearly indicate that this region of South America is dynamically complex.

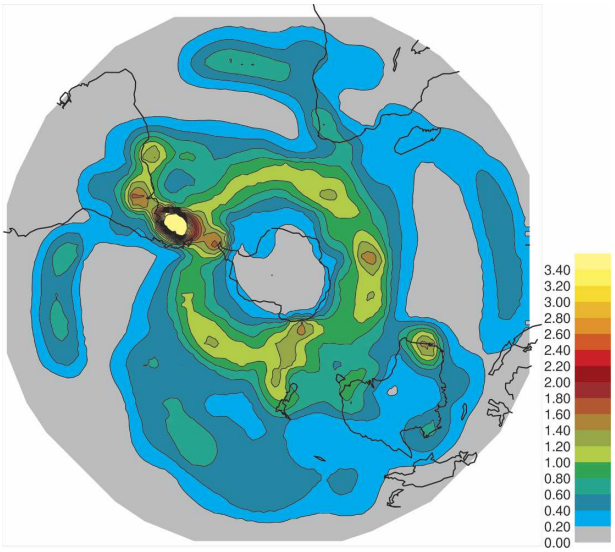

FIG. 12. Southern Hemisphere DJF (summer) ξ_{850} cyclogenesis over the whole hemisphere, number density per month per unit area (unit area as in Fig. 4).

The new feature is that off Brazil centered at 26°S. As discussed, for example, by Taljaard (1972), the systems move poleward and eastward from here along a region that corresponds to the southwestern flank of the lower-tropospheric subtropical anticyclone and the southern edge of the South Atlantic convergence zone (SACZ) cloud band. Similarly, in the Pacific near 150°W there is genesis also along the flank of the subtropical anticyclone and the South Pacific convergence zone (SPCZ) cloud band. In the western Indian Ocean, there is a corresponding but weaker feature extending southeastward from Madagascar. The subtropical genesis regions near western Australia and 180° lead to cyclones that are not very mobile. The winter genesis in the Pacific storm-track region is not present in summer. At higher latitudes the cyclogenesis is generally similar to that in winter, except that the genesis near Antarctica near 150°E, though still present, is much weaker.

6. Discussion and concluding comments

The use of ERA-40 data and modern computer variance and tracking techniques has enabled a detailed view of the Southern Hemisphere storm tracks to be attained. According to the technique and variable used, the details change somewhat, but the general picture remains similar. In the summer there is a rather circular high-latitude storm track. In winter the high-latitude storm track is more asymmetric, with a spiral from the Atlantic and Indian Oceans in toward Antarctica, and a subtropical jet–related lower-latitude storm track over the Pacific, again tending to spiral poleward. At all times of the year, maximum storm activity in the higher-latitude storm track is in the Atlantic and Indian Ocean regions. There the maximum activity is in the summer in the upper troposphere but generally in the winter in the lower troposphere. It is noteworthy that, unlike the Northern Hemisphere, the Southern Hemisphere winter storm track can appear weaker or stronger than that in the summer, depending on the diagnostic used. This closer similarity between the solsticial seasons is consistent with the small area of continental regions. The SST gradients (Figs. 1c,d) are very similar in the two seasons and are in fact slightly stronger in summer than winter between 35° and 55°S. Finally the summer storm track is a single, deep concentrated high-latitude entity, whereas the winter track has both upper subtropical and deep high-latitude components. Also, in agreement with others, and consistent with the thermal inertia of the largely ocean-covered surface, the Southern Hemisphere equinoctial season storm tracks tend to have similarity with those in the preceding seasons: autumn with summer, and spring with winter.

A detailed study based on feature tracking in winter has yielded a number of interesting results, in some cases giving more support to previous ideas and in other cases new ideas. Tracking of cyclonic features in ξ_{250} has emphasized the separation of, and interplay between, the polar and subtropical jet storm tracks in winter. This has recently been discussed by Nakamura and Shimpo (2004), who have stressed the trapping of wave activity by the strong subtropical jet and the consequent lack of leakage into the polar storm track in the Pacific. In vorticity, and even more in $\theta_{PV=2}$, the maximum average intensities are associated with the subtropical track. However, the polar track dominates when using geopotential height, for example. The track densities, but not the intensities, suggest a spiral from the subtropics in the Pacific to higher latitudes in the Atlantic and Indian Oceans with a strong split from 90° to 270°E.

The genesis of lower-tropospheric cyclonic systems in the South American sector occurs near 30° and 45°S as well as on the Antarctic Peninsula. These same regions were present in the cyclogenesis results of Simmonds and Keay (2000, their Fig. 3a) and Chung (1977) and where suggested by the extended EOF analysis of Vera et al. (2001). The poleward two of these regions appear to be mostly associated with the decay of systems upstream of the Andes and the Peninsula and their regeneration downstream of the mountains. The equatorward genesis region has been shown here to be associated with an upstream region of intense but shallow cyclonic systems on the subtropical jet, and individual

low-level genesis events can usually be linked to particular upper-level systems. The low-level jet on the eastern side of the Andes may be important in providing moisture that enhances the development process. There is a strong similarity with the separate northern and southern Rockies genesis regions shown for the Northern Hemisphere in Hoskins and Hodges (2002, their Fig. 6c). Also, intriguingly, anticyclogenesis regions are found some 5°–10° poleward of each cyclogenesis region in both hemispheres. In longitude there are sequential regions of anticyclolysis and cyclolysis on the upslope, anticyclogenesis over the mountains, and cyclogenesis on the downslope. These features appear to be consistent with simple vortex-stretching ideas for flow over topography, but further research is required to fully understand the mechanisms behind these distributions.

Isolating the ξ_{850} systems from the genesis maxima enabled the production of the overlapping plate reconstruction of the lower-tropospheric storm track given in Fig. 7. This is suggestive of a sequence of cyclones going through their life cycles with the upper-tropospheric storm track giving the genesis in the next region through downstream development and subsequent deep growth in favorable regions. The overlapping plate plus upper-track reconstruction gives a striking picture of the storm-track spiral from Australia to southern South America and then from the three genesis regions across the Atlantic and Indian Oceans and around Antarctica in the extreme southern Pacific.

The Pacific winter storm track appears here rather more clearly in vorticity tracking than in Eulerian variances and perhaps than in previous discussions. It is coherent in depth and in geographical space, from near 30°S off eastern Australia to 40°–45° upstream of South America.

As highlighted in, for example, the growth/decay of winter ξ_{850} cyclonic systems (Fig. 5b), the general picture is one of growth equatorward of 50°S and decay poleward of 60°S. This is similar to the picture given by Simmonds et al. (2003) for surface pressure systems, but the zero line is slightly more equatorward. Figure 8 shows that most of the systems that die near Antarctica have spiraled in from higher latitudes. However, as stressed by Simmonds et al. (2003) and shown in Figs. 5c and 8a, some cyclones are generated near Antarctica. In particular, ξ_{850} cyclonic systems are generated over the ice near 150°E. This region of enhanced genesis does not appear to have been discussed previously. One possible suggestion for its existence is that the lower-tropospheric systems decay upstream of 150°E as they move eastward by the side of the extremely steep coastal topography of east Antarctica and that it is here that they first get the possibility of a significant influx of cold air in depth. They appear at their most prevalent during the winter season when the SH has its greatest asymmetry in storm-track activity and more storms spiral into the upstream region. This situation is also apparent at 500 hPa (Figs. 5e,d), indicating that many of these systems have some depth to them at initiation and that they form in association with an existing system. This physical argument is in contrast to the focus on katabatic flows that have been proposed as being important for the short-lived mesocyclones (e.g., Bromwich and Parish 1998) that do not pass the acceptance criteria used in this study.

Inatsu and Hoskins (2004), partly inspired by the results discussed in this paper, used atmospheric GCM experiments with changed SST or topography to isolate the reasons for the asymmetries of the winter SH storm track. In the upper troposphere, the major determinant of the narrow, extended maximum in synoptic timescale eddy kinetic energy in the Atlantic and Indian Oceans and the sudden end upstream of New Zealand was found to be a stationary Rossby wave train forced by tropical convection asymmetries. The wave source in the Indian Ocean region was associated with the outflow from the monsoon there. The major determinant of the intensity of the lower-tropospheric storm track in the Atlantic and Indian Oceans in the GCM was found to be the enhanced midlatitude SST gradients there. The important role suggested for the Andes in the diagnostics presented here is consistent with the GCM result that without the Andes the Atlantic part of the storm track was considerably weaker. The cyclogenesis region found near South Africa is also consistent with the weaker storm track found in the GCM with the topography there removed. The spiral nature of the lower-tropospheric storm track was maintained in the GCM experiments if either the tropical or midlatitude SST asymmetries were retained. The former is consistent with the importance of the upper-tropospheric spiral storm track in creating the linkage between the overlapping plates of the lower-tropospheric storm track in Fig. 7a. The latter raises again the notion that there may be a positive feedback between the storm track and the SST gradients: the storm track leads to surface winds that drive the currents that lead to SST gradients, and these may be favorable for the storm track. If this coupled perspective is valid, the basic driving of the asymmetric SH winter storm track structure in both the upper and lower troposphere is by the asymmetries in tropical convection.

One interesting aspect of the summer ξ_{850} tracking is the genesis of eastward-moving cyclonic systems near the tropic of Capricorn off Brazil, in the central Pacific

and, to a lesser extent, off Madagascar. The former is important for the summer rain in southern Brazil. In each ocean basin, the systems move along the southwest flanks of the subtropical anticyclones and contribute to the "convergence zone" cloud bands seen in these regions.

This summer low-latitude discussion supports the picture given by Taljaard (1972). More generally, one of the outcomes of this paper is a confirmation of the remarkably high quality deductions about the nature and structure of Southern Hemisphere storm tracks made by earlier researchers, such as Taljaard (1972), on the basis of very limited amounts of data. (Note that a complete set of results from this study for all fields and all seasons is available online at www.nerc-essc.ac.uk/~kih/AMIP2/era40_results.html.)

Acknowledgments. The authors thank ECMWF for making the ERA-40 data available. They would also like to express their appreciation of comments made on an earlier draft by Hugo Berbery, John Turner, and Carolina Vera. The authors would also like to acknowledge the comments of the two anonymous referees that led to improvements in this paper.

APPENDIX

Pre– and Post–Satellite Comparison

A larger degree of uncertainty in the representation of weather systems can be seen between different reanalyses in the SH when contrasted with the NH (Hodges et al. 2003). This same comparison has been performed for ERA-40. In general the climatological results and aspects of the storm tracks presented in this paper are robust between the different reanalyses as well as between the satellite and presatellite periods although there are some differences in detail.

The study of Bengtsson et al. (2004) has highlighted the significant changes in atmospheric properties such as integrated water vapor, tropospheric temperature, and vertically integrated kinetic energy with the introduction of the satellite observing systems. Comparison of MSLP between Faraday Station on the western side of the Antarctic Peninsula and ERA-40 shows excellent agreement back to 1979, differences of several hectopascals in the period 1974–79, and much larger differences before that (J. Turner 2004, personal communication). Such results raise the question of whether there are also differences in the tracking statistics between the presatellite and satellite periods and if this has any impact on the results presented here.

To explore the impact on our results of the introduction of the satellite observing systems, the same analysis has been performed on the presatellite (1958–78) and satellite periods (1979–2003) separately. Although some satellite data were available before 1979 from VTPR, the major change occurred around 1979. Figures A1a and A1b show distributions for the SH wintertime cyclones with respect to their maximum intensities based on MSLP and ξ_{850}, respectively, for the presatellite (1958–78) and satellite (1979–2003) periods for ERA-40 and the satellite period for the NCEP–NCAR reanalysis [the Department of Energy (DOE) reanalysis shows similar results]. This shows that the number of systems is generally higher in the earlier period but that the maximum intensities are higher in general in the later period for ERA-40. This is true for both variables and hence provides us with some confidence that this result is a consistent one. The difference between ERA-40 and NCEP for the satellite period is as large as the difference between the presatellite and satellite periods for ERA-40, indicating the relatively large uncertainty in the SH between reanalysis even though the same observations have been used.

The SH is dominated by the satellite data, which has increased dramatically in recent years, such that the ECMWF analyses and forecasts have improved significantly in recent years. This may explain the decrease in the number of storms and the increase in the mean intensities in the latter period. Before the introduction of the satellite data, the SH ERA-40 analyses will be more influenced by the GCM. Since model-generated storms tend to be smoother and longer lived, this results in more storms passing the selection criteria. Also, the model may be biased to weaker intensities than when it is better constrained in the latter period by the satellite observations. These results are reflected in the differences in the 2–6-day standard deviations of MSLP and ξ_{850} shown in Figs. A1c and A1d, respectively, particularly for $\xi_{850,}$ which shows a reduction in activity in the latter period throughout the storm-track region although with some increase close to the Antarctic coast. This is perhaps less clear for MSLP, but it should be remembered that the Eulerian variances are a combination of the distribution of storms and their properties. These spatial variations are also apparent in the tracking statistics (track density and mean intensity; not shown). These indicate in general more systems in the main storm-track region with some reduction around the Antarctic coast in the former period and more intense storms in the latter period.

The final conclusion from our extensive comparison between different reanalyses and the ERA-40 presatellite and satellite periods is that although there are

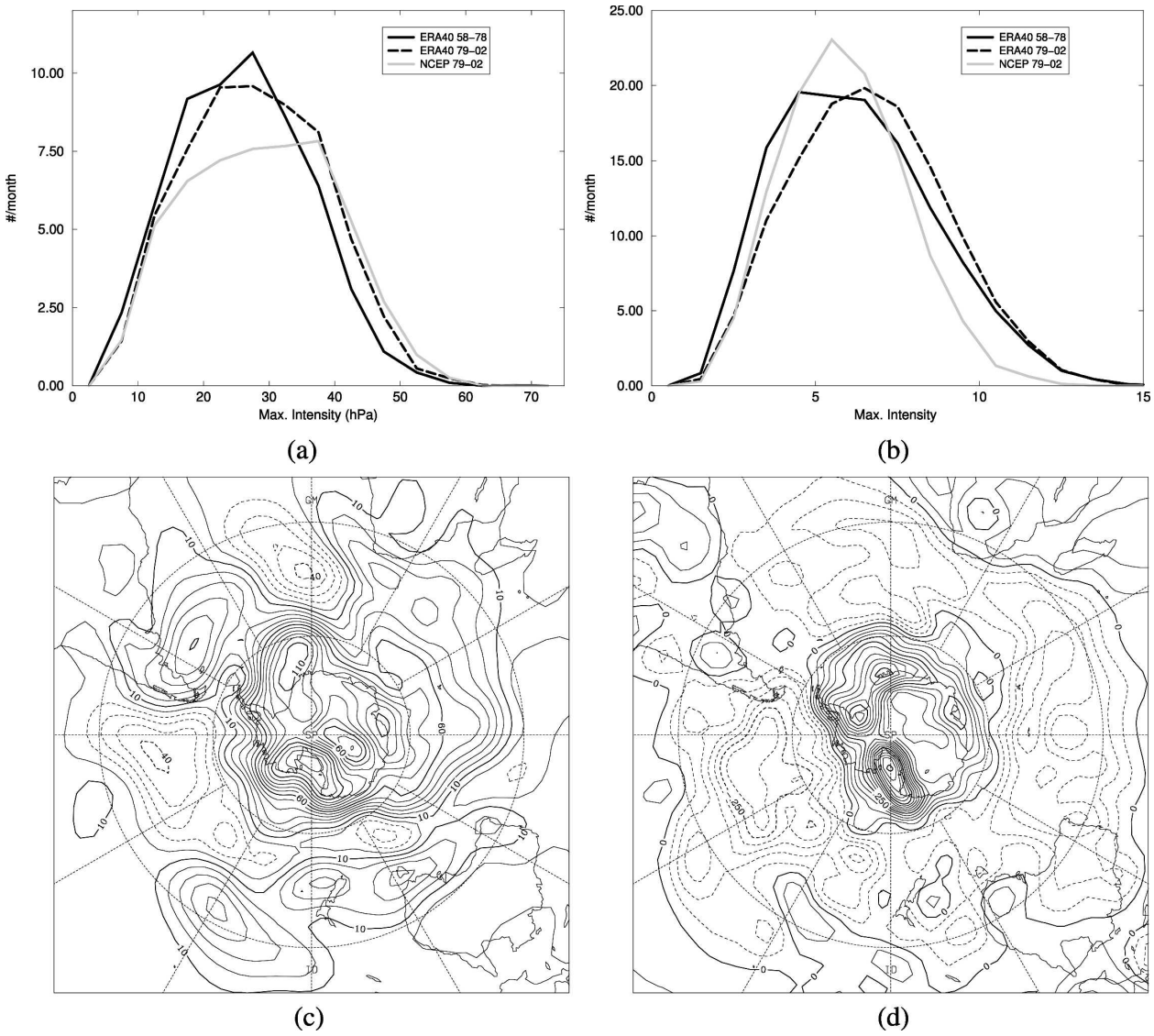

FIG. A1. Differences in storm-track activity for the winter (JJA) period between the presatellite (1958–78) period and the satellite (1979–2002) period. (a) Distribution of cyclonic storms (number per month) with respect to their maximum intensity for MSLP; absolute intensity (in hPa) relative to removed background. (b) Distribution of cyclonic storms (number per month) with respect to their maximum intensity for ξ_{850}; absolute intensity in 10^{-5} s^{-1} relative to removed background. (c) Difference in the 2–6-day standard deviation (Pa) for MSLP (satellite minus presatellite periods). (d) Difference in the 2–6-day standard deviation (10^{-5} s^{-1}) for ξ_{850} (satellite minus presatellite periods).

differences in the number and intensities of storms, the aspects of the SH storm tracks discussed here are robust.

REFERENCES

Anderson, D., K. I. Hodges, and B. J. Hoskins, 2003: Sensitivity of feature-based analysis methods of storm tracks to the form of background field removal. *Mon. Wea. Rev.,* **131,** 565–573.

Bengtsson L., S. Hagemann, and K. I. Hodges, 2004: Can climate trends be calculated from reanalysis data? *J. Geophys. Res.,* **109,** D11111, doi:10.1029/2004JD004536.

Berbery, E. H., and C. S. Vera, 1996: Characteristics of the Southern Hemisphere winter storm track with filtered and unfiltered data. *J. Atmos. Sci.,* **53,** 468–481.

——, and V. R. Barros, 2002: The hydrological cycle of the La Plata basin in South America. *J. Hydrometeor.,* **3,** 630–645.

Bromwich, D. H., and T. R. Parish, 1998: Meteorology of the Antarctic. *Meteorology of the Southern Hemisphere, Meteor. Monogr.,* No. 49, Amer. Meteor. Soc., 175–200.

Carlton, A. M., 1981: Monthly variability of satellite derived cyclonic activity for the Southern Hemisphere winter. *J. Climatol.,* **1,** 21–38.

Carrasco, J. F., D. H. Bromwich, and A. J. Monaghan, 2003: Dis-

tribution and characteristics of mesoscale cyclones in the Antarctic: Ross Sea eastward to the Weddell Sea. *Mon. Wea. Rev.,* **131,** 289–301.

Chang, E. K. M., 1999: Characteristics of wave packets in the upper troposphere. Part II: Seasonal and hemispheric variations. *J. Atmos. Sci.,* **56,** 1729–1747.

Chung, Y., 1977: On the orographic influence and lee cyclogenesis in the Andes, the Rockies and the East Asia Mountains. *Arch. Meteor. Geophys. Bioklimatol.,* **26A,** 1–12.

Fouquart, Y., and B. Bonnel, 1980: Computations of solar heating of the Earth's atmosphere: A new parameterization. *Beitr. Phys. Atmos.,* **53,** 35–62.

Frederiksen, J. S., 1984: The onset of blocking and cyclogenesis in Southern Hemisphere synoptic flows: Linear theory. *J. Atmos. Sci.,* **41,** 1116–1131.

Hodges, K. I., 1995: Feature tracking on the unit sphere. *Mon. Wea. Rev.,* **123,** 3458–3465.

——, 1996: Spherical nonparametric estimators applied to the UGAMP model integration for AMIP. *Mon. Wea. Rev.,* **124,** 2914–2932.

——, 1999: Adaptive constraints for feature tracking. *Mon. Wea. Rev.,* **127,** 1362–1373.

——, B. J. Hoskins, J. Boyle, and C. Thorncroft, 2003: A comparison of recent reanalysis datasets using objective feature tracking: Storm tracks and tropical easterly waves. *Mon. Wea. Rev.,* **131,** 2012–2037; Corrigendum, **132,** 1325–1327.

Holton, J. R., 1992: *An Introduction to Dynamic Meteorology.* 3d ed. Academic Press, 511 pp.

Hoskins, B. J., and P. D. Sardeshmukh, 1984: Spectral smoothing on the sphere. *Mon. Wea. Rev.,* **112,** 2524–2529.

——, and P. Berrisford, 1988: A potential vorticity perspective on the storm of 15–16 October 1987. *Weather,* **43,** 122–129.

——, and K. I. Hodges, 2002: New perspectives on the Northern Hemisphere winter storm tracks. *J. Atmos. Sci.,* **59,** 1041–1061.

Hurrell, J. W., H. van Loon, and D. J. Shea, 1998: The mean state of the troposphere. *Meteorology of the Southern Hemisphere, Meteor. Monogr.,* No. 49, Amer. Meteor. Soc., 1–47.

Inatsu, M. and B. J. Hoskins, 2004: The zonal asymmetry of the Southern Hemisphere winter storm track. *J. Climate,* **17,** 4882–4891.

Lee, S., and I. M. Held, 1993: Baroclinic wave packets in models and observations. *J. Atmos. Sci.,* **50,** 1413–1428.

Lott, F., and M. J. Miller, 1997: A new subgrid-scale orographic drag parameterization: Its formulation and testing. *Quart. J. Roy. Meteor. Soc.,* **123,** 101–127.

Mechoso, C. R., 1980: The atmospheric circulation around Antarctica: Linear stability and finite-amplitude interactions with migrating cyclones. *J. Atmos. Sci.,* **37,** 2209–2223.

Mlawer, E. J., S. J. Taubman, P. D. Brown, M. J. Iacono, and S. J. Clough, 1997: Radiative transfer for inhomogeneous atmospheres: RRTM, a validated correlated-k model for the longwave. *J. Geophys. Res.,* **102D,** 16 663–16 682.

Nakamura, H., and A. Shimpo, 2004: Seasonal variations in the Southern Hemisphere storm tracks and jet streams in a reanalysis dataset. *J. Climate,* **17,** 1828–1844.

Rao, V. B., A. M. C. do Carmo, and S. H. Franchito, 2002: Seasonal variations in the Southern Hemisphere storm tracks and associated wave propagation. *J. Atmos. Sci.,* **59,** 1029–1040.

Simmonds, I., and R. J. Murray, 1999: Southern extratropical cyclone behavior in ECMWF analyses during the FROST special observing period. *Wea. Forecasting,* **14,** 878–891.

——, and K. Keay, 2000: Mean Southern Hemisphere extratropical cyclone behavior in the 40-year NCEP–NCAR reanalysis. *J. Climate,* **13,** 873–885.

——, ——, and E. Lim, 2003: Synoptic activity in the seas around Antarctica. *Mon. Wea. Rev.,* **131,** 272–288.

Simmons, A. J., and B. J. Hoskins, 1979: The downstream and upstream development of unstable baroclinic waves. *J. Atmos. Sci.,* **36,** 1239–1254.

——, and J. K. Gibson, 2000: The ERA40 Project plan. ERA40 Project Report Series No. 1, ECMWF, Shinfield Park, Reading, United Kingdom, 63 pp.

Sinclair, M. R., 1994: An objective cyclone climatology for the Southern Hemisphere. *Mon. Wea. Rev.,* **122,** 2239–2256.

——, 1995: Climatology of cyclogenesis for the Southern Hemisphere. *Mon. Wea. Rev.,* **123,** 1601–1619.

——, 1996: A climatology of anticyclones and blocking for the Southern Hemisphere. *Mon. Wea. Rev.,* **124,** 245–263.

Streten, N. A., and A. J. Troup, 1973: A synoptic climatology of satellite observed cloud vortices over the Southern Hemisphere. *Quart. J. Roy. Meteor. Soc.,* **99,** 56–72.

Taljaard, J. J., 1972: Synoptic meteorology of the Southern Hemisphere. *Meteorology of the Southern Hemisphere, Meteor. Monogr.,* No. 35, Amer. Meteor. Soc., 139–213.

Tiedtke, M., 1989: A comprehensive mass flux scheme for cumulus parameterization in large-scale models. *Mon. Wea. Rev,* **117,** 1779–1800.

Trenberth, K. E., 1991: Storm tracks in the Southern Hemisphere. *J. Atmos. Sci.,* **48,** 2159–2178.

——, and K. C. Mo, 1985: Blocking in the Southern Hemisphere. *Mon. Wea. Rev.,* **113,** 3–21.

Turner, J., G. J. Marshall, and T. A. Lachlan-Cope, 1998: Analysis of synoptic scale low pressure systems within the Antarctic Peninsula sector of the circumpolar trough. *Int. J. Climatol.,* **18,** 253–280.

van Loon, H., 1967: The half-yearly oscillation in middle and high southern latitudes and the coreless winter. *J. Atmos. Sci.,* **24,** 472–486.

Vera, C. S., P. K. Vigiarolo, and E. H. Berbery, 2001: Cold season synoptic-scale waves over subtropical South America. *Mon. Wea. Rev.,* **130,** 684–699.

White, P., 2000: IFS documentation Part III: Dynamics and numerical procedures (CY21R4). Meteorological Bulletin M1.6/4, ECMWF, Shinfield Park, Reading, United Kingdom, 36 pp.